J. Phys. B: At. Mol. Opt. Phys. **31** (1998) 4267–4282. Printed in the UK PII: S0953-4075(98)93252-7

Quantized momentum mechanics of inelastic and reactive collisions: the role of energy and angular momentum constraints

Nicholas A Besley, Anthony J McCaffery, Mark A Osborne and Zaid Rawi

School of Chemistry, Physics and Environmental Science, University of Sussex, Falmer, Sussex, UK

Received 14 April 1998, in final form 31 July 1998

Abstract. In addition to the quantized molecular structure that constrains the kinematics of atom–molecule collision, constraints arising from energy and angular momentum (AM) conservation strongly influence the magnitude and probability distribution of rotational transfer due to collisions. However, once the nature of these constraints is established, it is possible to predict quantitatively, using quantized momentum mechanics, the outcome of inelastic and reactive collisions. The existence of these constraints is most clearly portrayed in plots of relative velocity (v_r) versus final rotational AM (j'). These represent channel opening under the conditions: (i) energy conservation, (ii) simultaneous energy and angular momentum conservation, the latter via a specified maximum effective impact parameter b_n^{max} and (iii) angular momentum conservation via this same b_n^{max}. b_n^{max} is generally set to be the half bond length (HBL) of the diatomic, as suggested by experimental and theoretical considerations. Each of these conditions may constrain the rotational transfer process. The v_r–j' plots also give indications of conditions under which backward or forward scattering will occur and when long-lived complexes will form. For sharply defined velocity distributions, scattering angle peaks are readily calculated and these agree well with experimental data. When energy constraints dominate, the value of b_n^{max} may be less than HBL and this reduced value may be obtained from the kinematic equations. This permits wider usage of the AM theory of rotational transfer. AM constraints effectively reduce the number of channels that appear to be accessible from energetic considerations. The v_r–j' plots may also be used to analyse reactive collisions and inelastic processes in polyatomic molecules for data in which the angular momentum change is directed principally along one of the molecule's inertial axes.

1. Introduction

In recent publications [1], we have outlined a simple kinematic model for molecular collisions and have used this to interpret the results of modern collision and reaction dynamics experiments. The model utilizes Newtonian mechanics of linear-to-linear, or of linear-to-angular momentum interconversion but this is modified by the known internal quantum state structure of the molecule. Thus it has the intuitive and visual appeal of classical mechanics, while retaining essential quantum features. Calculations based on this model accurately reproduce results obtained from state-resolved molecular dynamics experiments. They require only modest computational resources and use readily available data such as atomic masses, bond lengths and velocity distributions. This gives the model considerable predictive power.

0953-4075/98/194267+16$19.50

The model focuses on the disposal of momentum via vector relationships. Experimental results demonstrate [1] that constraints arising from the molecule's internal quantum structure are imposed on the otherwise classical behaviour. We have proposed that quantum-constrained kinematics controls the momentum exchange process and introduce the term *quantized momentum mechanics* (QMM) to describe the mechanics of the interaction. The existence of this hybrid quantal–Newtonian mechanics was deduced from the analysis of state-, velocity- and angle-resolved inelastic scattering experiments [1]. The method is also an accurate predictor of quantum state distributions in diatomic molecule products following *reactive* collisions [2]. QMM expresses the dominance of *vector* relationships in the interconversion of linear and angular momentum in a sense not previously recognized though is implicit in the work of Herschbach and co-workers [3]. Bosanac [4] has shown that the incorporation of uncertainty as 'Newton's fourth postulate' allows quantum relationships to be derived from classical mechanics and this could be seen as providing theoretical justification for the model.

QMM is the basis of the angular momentum (AM) model of rotational transfer (RT) that we introduced recently [5]. In this, RT is formulated as the joint probability $p(\Delta E, \Delta j)$ of two events, one the conversion of kinetic energy of relative motion to rotational energy and the other, the conversion of relative linear momentum into rotational angular momentum. These two probabilities were taken to be independent and thus $p(\Delta E, \Delta j) = p(\Delta E)\, p(\Delta j)$. We have presented evidence that the vector process (i.e. $p(\Delta j)$) controls the probability of RT, within limits set by energy conservation. Here we demonstrate both the separability of energy and AM factors and the dependence on $p(\Delta j)$.

In the AM model of RT [5], collisional state change entails the conversion of linear momentum of relative motion into internal (rotational) AM, vibrational momentum and/or recoil momentum. This process takes place under constraints imposed by conservation of total energy and of total angular momentum as well as the quantum constraints that are a consequence of the quantized energy and AM states of the molecule. Here we examine the circumstances under which one or the other of the constraints on energy or AM becomes dominant. Total energy and AM must be conserved in any collisional event but the manner in which this is achieved, in for example the balance between transfer and recoil, can differ markedly depending on a number of factors.

The purpose of this publication is to demonstrate that consideration of the kinematic conditions under which one or other of the conservation requirements becomes dominant, leads to a valuable physical insight and greatly enhances our capacity to predict collision outcomes. Constraints based on AM conservation for example, identify circumstances under which certain channels are effectively closed for a given relative velocity though formally open in an energetic sense. Constraints based on energy conservation may, in some circumstances, lead to a reduction of channels apparently open on the basis of available AM. This is manifest as a reduced effective impact parameter in AM theory which fits [5, 6] to experimental data and hence diminished RT. The existence of AM constraints in inelastic collisions has been discussed by Derouard and Sadeghi for the atom–diatom case [7] and by Flynn and co-workers in the case of atom–linear triatomic encounters [8]. The possibility of competition between energy and AM constraints in reactive collisions has been addressed by Kalogerakis and Zare [9].

The operation of energy (E) and AM constraints is best quantified in plots of relative velocity versus final molecular rotational AM as illustrated below, where graphs are shown for reactive as well as non-reactive collisions. We also demonstrate that state-to-state scattering patterns may be inferred for both inelastic and reactive collisions on the basis of threshold interconversion relations and this may be quite precise when the velocity

distribution is sharply defined. Thus the velocity–j' plots, which are presented here for the first time, contain considerable insight into collisional processes and constitute a useful first step in a detailed analysis of collisional data in terms of the kinematics.

2. Angular momentum and energy constraints

Collision-induced rotational state change is assumed to result from the conversion of linear to angular momentum at the repulsive wall of an ellipsoidal intermolecular potential. The collisions are assumed to be impulsive and thus only the component of linear momentum normal to the ellipsoid surface will change during the momentum transfer process. The collision energy in an atom–diatomic molecule encounter is

$$E_c = \mu v_r^2/2 \tag{1}$$

where v_r is the relative speed of the colliding pair and μ is the reduced mass of the system. The orbital angular momentum, l, available for transfer into molecular rotation is

$$l = \mu v_n b_n \tag{2}$$

where v_n is the normal component of relative velocity and b_n is the effective impact parameter (or 'torque arm'), which is given by the distance from the centre of the ellipse to the surface normal at the point of impact [10].

For an initially non-rotating diatomic, conservation of angular momentum requires that

$$l = j' + l' \tag{3}$$

where j' and l' are the final values of rotational and angular momentum, respectively. Conservation of energy and the component of momentum parallel to the ellipse surface at the point of impact requires that

$$\frac{l^2}{2\mu b_n^2} = \frac{j'^2}{2I} + \frac{l'^2}{2\mu b_n^2} \tag{4}$$

where I is the moment of inertia of the molecule.

The j' channel opening or *threshold* condition may be expressed as [11, 12]

$$j' = \frac{2I\mu v_{th} b_n^{max}}{\mu (b_n^{max})^2 + I}. \tag{5}$$

Here, v_{th} is the threshold relative velocity, b_n^{max} is the maximum available b_n value. The quantity b_n^{max} is a central parameter in the AM theory of rotational transfer (RT) [5, 6]. Fits to experimental data [6] reveal that b_n^{max} frequently is close to the half bond length (HBL) of the diatomic molecule involved in the inelastic collision, though in certain instances, significant reductions from this value are found.

Rotationally inelastic transitions generally absorb only a small fraction of the initial relative linear momentum available under normal experimental conditions and hence scattering is predominantly in a forward direction. In such a case the threshold condition is given by an expression simpler than that of equation (5), namely

$$j' = \mu v_{th} b_n^{max}. \tag{6}$$

In this formulation, energy conservation requirements are met by the scattered portion of the initial velocity which contributes to the second term on the right-hand side of equation (4). Under the condition that equation (6) holds (and forward scattering dominates most situations of linear-to-angular momentum conversion, in both reactive and non-reactive collisions), we have demonstrated [1], that the *perpendicular* component of initial velocity is that which

just opens the j' channel and the parallel component is scattered unused. Note that the terms parallel and perpendicular here refer to the surface element of the ellipsoid upon which the collision makes impact.

The threshold conditions for change of rotational quantum number resulting from interconversion of *energy* (when all the collision energy becomes rotational energy) may be expressed as follows, for an initially rotating molecule (the corresponding expression for an initially non-rotating molecule may be obtained from this expression by setting $j_i = 0$),

$$\Delta j' = j_i + \frac{\sqrt{(2Bj_i)^2 + 2B\mu v_r^2}}{2B}. \tag{7}$$

In equation (7), B is the rotational constant and j_i is the initial rotational state.

We note that on collision, the *maximum* theoretical transferable momentum is twice the initial value (i.e. $2p_i$) when the relative velocity vector returns along its initial path (representing 180° or total backscattering). Collision-induced quantum state change will modify this due to the requirements of energy conservation as expressed in equation (5). Equations (5)–(7) therefore represent channel opening or threshold conditions under circumstances of

(i) simultaneous energy *and* AM conservation in the RT process (equation (5)), with use of maximum effective torque arm, b_n^{max}, and characterized by transfer of momentum *greater* than the initial momentum p_i;
(ii) AM conservation with full utilization of initial momentum p_i and of maximum torque arm b_n^{max}. Energy conservation in this case is met through the l' component of equation (6) and scattering is in a forward direction.
(iii) Energy conservation (equation (7)). When this provides the dominant constraint, AM conservation may be achieved by a reduction in b_n^{max} (discussed in detail below).

In terms of quantum state-resolved scattering, equation (5) represents the threshold for maximum backward scattering and equation (6) that for the onset of forward scattering. Since each of the equations is expressed in terms of relative velocity and other known quantities, knowledge of the relative velocity distribution would allow us to infer state-to-state scattering patterns for each final j' state. Relatively few angular distributions of this kind have been measured, particularly sparse being state-resolved data in which backward scattering is significant. Nevertheless, it is instructive to illustrate how scattering may be inferred from kinematic considerations alone and to demonstrate the predictive power of simple kinematic relationships.

2.1. Velocity–rotational AM plots

The clearest indication of the operation of constraints due to energy or AM considerations is seen when equations (5)–(7) are plotted as (post-collision) rotational quantum number, j' (Δj if the molecule was rotating prior to collision) versus relative velocity v_r. These plots are collision system specific and represent the threshold conditions of relative velocity for each j channel under optimal conditions for conversion. As is apparent from the form of equations (5)–(7), they are principally determined by the kinematics of the collision process.

We demonstrate below that these plots may be used to analyse limits on the outcome of both non-reactive and reactive collisions (when the product species is a diatomic molecule). Input data are readily available, consisting of atomic masses, bond lengths, rotational constants and relative velocities. The method may be applied to systems for which there are detailed experimental results or in circumstances where such knowledge exists. The extent to which the operation of energy or AM constraints may influence the rotational channels

that are accessible in an inelastic or reactive collision is best illustrated by example and we give below a number of instances where the operation of one or other of these constraints has a demonstrable influence on the collision outcomes.

3. Atom–diatom rotationally inelastic collisions

We illustrate the basic principles of the analysis using two well known limiting cases of heavy and light diatomics (I_2 and Li_2) inelastically colliding with heavy and light rare-gas atoms (Xe and He). Figures 1 and 3 plot v_r versus j (in units of $\hbar$) for these diatomics with He and with Xe as collision partners. In these graphs, the molecule is considered to be initially non-rotating and thus j' represents the change of AM that results from the collision. The effects which arise when initially $j_i > 0$ are subtle but far reaching and we discuss this topic in detail later in the paper.

Note that specific values of b_n^{max} were chosen in calculating the data points from equations (5) and (6) for the graphs of figures 1 and 3. The value chosen was generally the half bond length (HBL) of the diatomic molecule. This value is frequently found to be the maximum *effective* impact parameter from AM theory fits to RT data [6] and from molecular beam scattering experiments [13]. Thus in this kinematic model, the role of the intermolecular potential is implicitly recognized in the form of the dimensions of the repulsive wall at the zero contour, which is reasonably well approximated by the size of the diatomic molecule. Torque is generated from the potential via its angular dependence and is proportional to $-dV/d\Theta$. Bosanac [10] calculated that this variation is sufficient to generate rotational AM change *only* at the repulsive wall.

The focus here is on conditions that effectively lead to the opening of individual j' channels and in this the representation of b_n^{max} by HBL aids rule-of-thumb visualization and is found to give zero-order or better accuracy in predicting the outcome of collisions. However, setting b_n^{max} to this value might be seen as an overly severe restriction. In principle, the value of b_n^{max} may be increased until the conversion rate through equation (6) matches that of equation (7) and if we were considering the *energy* interchange between collision velocity and internal rotational energy, we might be tempted to do so. The essence of the model used here is that linear-to-angular momentum conversion is the controlling mechanism of RT and that b_n^{max} is the *effective* torque arm in this process. This is the basis of our original model [5] and its predictive power has been demonstrated both theoretically and experimentally. Here our focus is on the constraints that arise when energy and AM conversion occur in inelastic and reactive events according to this model. It will be seen that genuine new insights are obtained into collision processes and a predictive capability that is absent in other formulations.

3.1. I_2–rare-gas collisions

Plots of equations (5)–(7) for the collision system I_2–He are shown in figure 1(*a*) (along with those for I_2–Xe in figure 1(*b*)). Figure 1 demonstrates that equations (5)–(7) convert relative velocity to rotational AM at very different rates.

Equation (7) constitutes the fastest rate of velocity–j'-value interconversion and indicates that j' values in excess of $100\hbar$ might be observable on the grounds of energetics alone. We refer to this as the E-conservation plot to distinguish it from the graph of equation (6), which is designated as A-conservation. Equation (5) will be described as the $(E + A)$-conservation plot. As is apparent from figure 1, the $(E + A)$- and the A-conserving relations are considerably more restrictive for these systems than is the E-

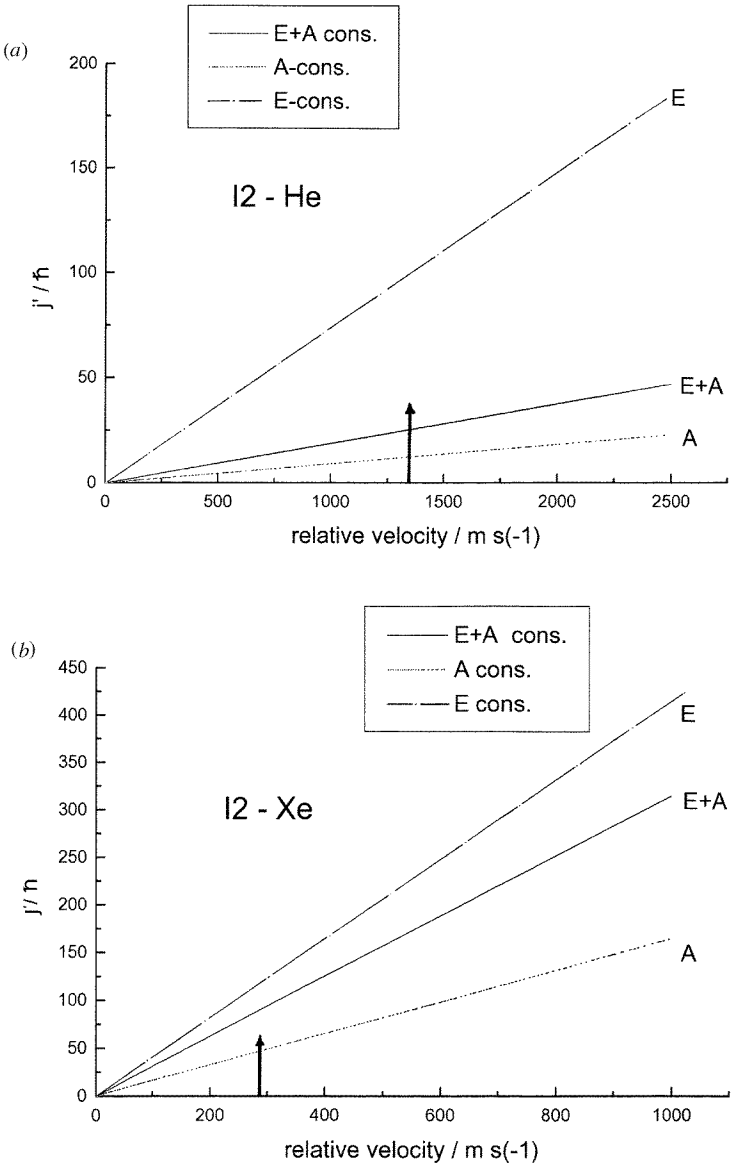

Figure 1. Plot of relative velocity (in m s^{-1}) versus final state rotational quantum number (j' in units of $\hbar$) for I_2–He (*a*) and for I_2–Xe (*b*). As discussed in sections 3 and 4, these represent channel opening or threshold conditions for energy conservation as quantified in equation (7); AM conservation, via equation (6) and simultaneous energy and AM conservation via equation (7). HBL of I_2 is used in calculating A- and the $(E+A)$-conservation j' as discussed in the text. The figure demonstrates that the maximum j' value observed experimentally will be constrained by the available AM, particularly in I_2–He. The plots therefore delineate regions that are allowed or forbidden for RT.

conserving equation. From $(E + A)$-conservation in I_2–He we might anticipate j' values of up to $50\hbar$ under typical experimental conditions and the A-conservation condition would limit this further to around $30\hbar$ or so. The extension of the v_r distribution well beyond

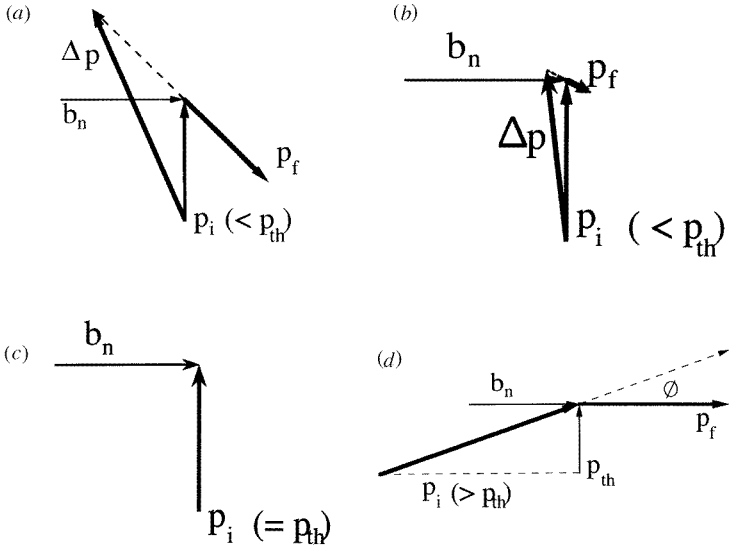

Figure 2. Vector representation of the fate of incident momentum $\boldsymbol{p}_{\mathrm{i}}$ and final momentum $\boldsymbol{p}_{\mathrm{f}}$ under different conditions of magnitude of $\boldsymbol{p}_{\mathrm{i}}$ and threshold momentum. In (*a*) and (*b*), $\boldsymbol{p}_{\mathrm{i}} < \boldsymbol{p}_{\mathrm{th}}$ and channel opening may only be achieved by backward scattering such that $\Delta\boldsymbol{p}$ (defined as $\boldsymbol{p}_{\mathrm{i}} - \boldsymbol{p}_{\mathrm{f}}) = \boldsymbol{p}_{\mathrm{th}}$. (*c*) represents the condition that $\boldsymbol{p}_{\mathrm{i}} = \boldsymbol{p}_{\mathrm{th}}$ with consequent formation of a long-lived complex. (*d*) is a representation of the most common condition of RT in which incident momentum is considerably larger than the channel opening momentum with forward scattering.

the most probable value prevents these limiting j' values from being more than estimates. Collision-induced RT in this system is predicted to be AM *constrained* therefore, as becomes evident on inspecting plots of the form of figure 1.

Experimental RT data on this system (note that the data and this discussion all refer to I_2 in its B $^3\Pi_0$ state) [7] show distinctive effects that have been attributed to momentum *deficiency*. Rotationally inelastic data on I_2 are generally obtained from samples in thermal cells at or close to room temperature. The most probable relative velocity is shown in figures 1(*a*) and (*b*) by an arrow on the velocity ordinate. For I_2–He this value is 1335 m s^{-1}. That RT in I_2–He is AM constrained has been known for a number of years and was influential in the development of AM-based scaling relations for RT [7]. Inelastic transfer is not seen to high Δj levels and state-to-state rate constants fall by more than two orders of magnitude by $\Delta j = 25\hbar$. Note that experimental data from non-rotating I_2 molecules are rarely available and initially we assume j' channel opening conditions to be similar to the appropriate Δj channels. This is not always the case however as we show below. An enhanced rate of fall-off (referred to as the *knee*) in the experimental data is observed from around $14\hbar$ and this is consistent with the A-conservation plot, given a relative velocity distribution which peaks at 1335 m s^{-1}. AM theory fits to I_2–He data [6] yield a $b_{\mathrm{n}}^{\max}$ very close to the HBL value of B-state I_2, a characteristic of AM constrained systems.

Figure 1(*b*) displays plots of equations (5)–(7) for I_2–Xe collisions. In this system the most probable relative velocity is 285 m s^{-1}, but the rate of conversion of velocity to AM is fast due to the increased reduced mass of the partners which now carry considerable amounts of linear momentum. The E- and the $(E + A)$-conserving relations now lie close together and predict that j' values in excess of $100\hbar$ might be observed. The A-conservation relation, on the other hand suggests that $60\hbar$ would be a more realistic limit given the constraint

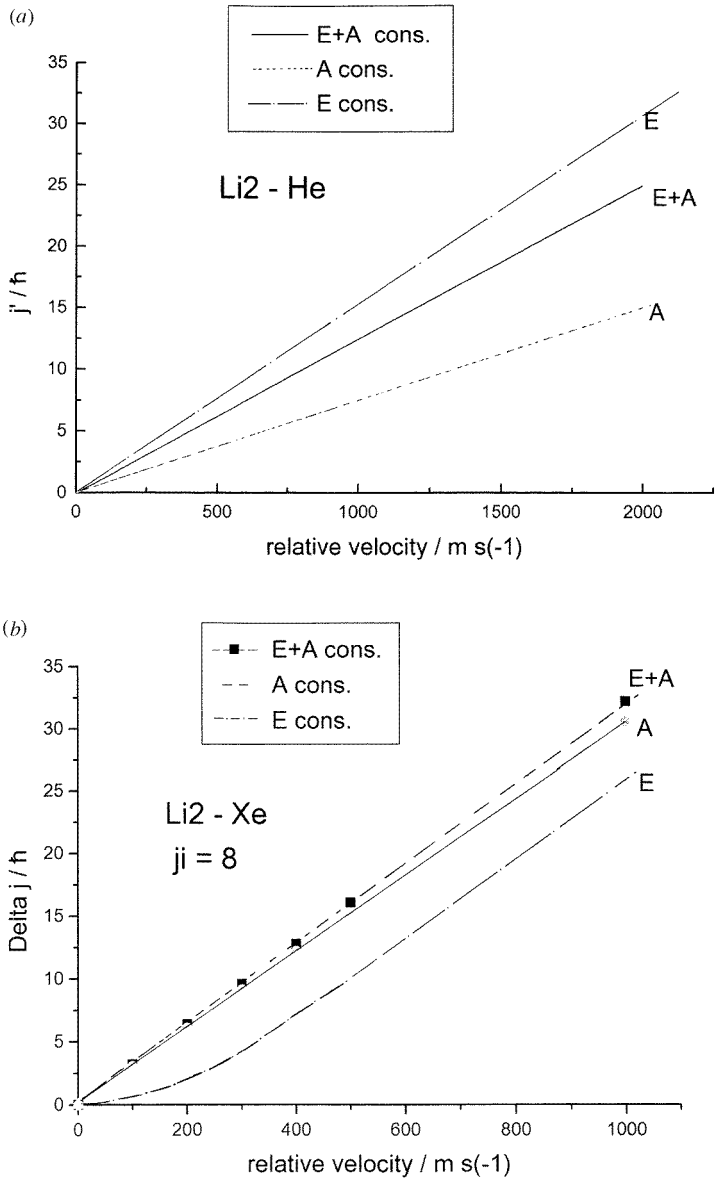

Figure 3. As for figure 1 but here the diatomic is Li_2. The Li_2–He system can be seen to be AM constrained in (*a*). In (*b*), the plot for Li_2–Xe is calculated for $j_i = 8$ and now the system becomes *energy* constrained. The effect of this is to reduce the length of the effective maximum torque arm.

provided by equation (6). Experimentally, this latter restriction appears to be the major influence though data from initially non-rotating molecules are unavailable. That AM is the constraining factor in published RT data is reflected in the recovery of close to HBL as b_n^{max} in AM theory fits to RT data in this system [6].

3.2. State-resolved scattering

Published state- and scattering-angle-resolved RT data [14] suggest that most rotationally inelastic processes are characterized by forward scattering and only when the angular momentum change is large in comparison to available relative momentum is backscattering observed. Although not immediately obvious, the predominant scattering direction is implicit in equations (5) and (6) and scattering angles may be predicted for a given system, particularly if the velocity distribution is sharply defined. We have recently demonstrated that scattering angles in forward scattering are accurately predicted from (quantum-constrained) kinematic considerations [1]. Here we show how the channel opening equations (5) and (6) and plots such as figures 1 and 3 allow scattering patterns to be inferred using I_2–He as the basis of the illustration.

Consider the $j' = 10$ channel in I_2–He in relation to the conservation plots (figure 1(*a*)). The energetic conditions for channel opening are reached at $v_r = 139.3$ m s^{-1}. However, in this model the channel remains effectively closed until $v_r = 528.5$ m s^{-1} when the process may be initiated by backward scattering. This follows from our knowledge that this velocity provides insufficient momentum by itself to open the $j' = 10$ channel. This level may only be reached (at this value of v_r) by a process in which the *change of momentum* is greater than that available from $v_r = 528.5$ m s^{-1}. This of course is a familiar situation in classical mechanics and in principle, momentum change $\Delta p = 2p_i$ is feasible (though not if RT occurs). The transferred momentum is the vector *difference* of initial and final momenta, i.e. $\Delta \boldsymbol{p} = \boldsymbol{p}_i - \boldsymbol{p}_f$ and an illustration of the mechanism by which transferred momentum may exceed the initial momentum through this relationship is given in figures 2(*a*) and (*b*). As these make clear, this process would be apparent in an experiment as backscattering (i.e. $\theta > 90^\circ$).

As relative velocity continues to increase, the scattering angle begins to move in a more forward direction until the threshold for channel opening via equation (6) is reached. At this point, 1040 m s^{-1}, for the case under consideration, the initial momentum is entirely used in opening the channel, the He atom becomes temporarily trapped and forms a long-lived complex. Depending on the lifetime of this complex, an isotropic scattering pattern might result as the long-lived species dissociates during rotation. The vector conditions for the trapped trajectory to occur are represented by figure 2(*c*).

At v_r values above the equation (6) channel opening condition the vector relationships are as shown in figure 2(*d*) and the relationship between scattering angle, initial velocity and v_r found by McCaffery and Wilson [1] may be expected to hold, i.e.

$$\sin\theta = v_{th}/v_r \tag{8}$$

where θ is the most probable scattering angle, v_{th} is the threshold, or channel opening velocity, and v_r is the relative velocity. This form of analysis allows accurate prediction of state-to-state scattering distributions which, for the case of sharply defined velocity distributions, may be very well defined.

Consider, for example, the I_2–He $j' = 10$ case for a velocity distribution sharply peaked around, say, 600 m s^{-1}. This is insufficient in momentum terms to open the $j' = 10$ channel through the A-conservation mechanism of equation (6), but sufficient through the (backscattering) $(E + A)$-conservation condition. For the case of a velocity distribution sharply peaked at 1500 m s^{-1} say, the forward scattering channel is now open and the peak scattering angle is calculated from equation (5) to be 44°. A thermal distribution of relative velocities at room temperature would yield a mixture of forward and backward scattering for $j' = 10$ with the majority of the flux in a forward direction since the most probable relative velocity is 1335 m s^{-1}. The relationship from which the scattering angle

is evaluated (equation (5)) has been shown to predict accurately all measured state-to-state rotationally inelastic scattering data [1] over a wide range of collision systems. Note that this discussion represents the situation at threshold or channel opening only. Higher relative velocities will also open particular channels via trajectories that generate torque arms which are shorter than the HBL maximum and contribute to the overall probability density for a given process.

We have predicted state-to-state scattering angular distributions for atom–diatom collisions on the basis of kinematic considerations along with knowledge of the quantum states that exist within the molecule. The forms of scattering predicted for different velocity distributions match well with the generic types that are observed experimentally and predicted theoretically [15]. We note, in particular, the *predictive* nature of the approach described here since state-resolved scattering angles have not been measured for I_2–He. The method is applicable to any collision system where a diatomic is the probed species since input data are readily available. For the forward scattering process (by far the most common in RT), the analysis by McCaffery and Wilson shows that this model predicts scattering angles accurately. This work also demonstrates that the threshold condition is of special significance in collision-induced processes. Note that the corollary of the observation in the first sentence of this paragraph is that we might not expect to obtain much information on the intermolecular potential from measurement of state-to-state scattering angles other than the dimensions of the diatomic that is being probed. This indeed was the conclusion of Hoffbauer *et al* [13] after a careful and lengthy study of $Cl_2 + Ar$. In a later section we explore the application of these methods in the case of *reactive* collisions.

3.3. Li_2–rare-gas collisions

Figure 3 displays plots of the three functions (equations (5)–(7)) for Li_2–He, Xe. These represent an alternative kinematic limit to the I_2 case considered above. Experimental RT data for this system are predominantly from $j_i > 0$ and, as we show later, this has a marked effect on the plot of the E-conservation relation. As is apparent from figure 3(*a*), the three plots are well separated only in the case of Li_2–He and in both collision systems when $j_i = 0$ the predominant constraint is provided by the A-conserving relation. Figure 3(*b*) shows the three conservation relations plotted for Li_2–Xe but now equation (7) is calculated for the case $j_i = 8$ (for which extensive experimental RT data exist [16]). Thus the ordinates become v_r versus Δj. It is seen that there is now pronounced curvature in the E-conservation plot at low v_r, which now lies below the A-conservation equation. Thus the process is dominated by an *energy* constraint.

It is interesting to speculate on how this energy constraint might be manifested. Since the v_r values are set by experimental or theoretical conditions, the only mechanism by which energy conservation requirements may be met is via reduction in the effective torque arm below the HBL value. It is straightforward to calculate the b_n^{max} value that would be required to meet E-conservation for the lowest of the inelastic processes and thus make all Δj transitions allowed. For the case of Li_2–Xe this is 0.56 Å for $\Delta j = 2$ from $j_i = 8$. The corresponding values for Li_2–Ar, Ne, all of which exhibit the energy constraint illustrated for Li_2–Xe, are 0.59 and 0.65 Å, respectively. For Li_2–He, $j_i = 8$, AM constraints continue to dominate though as j_i increases the trend towards E-constraint becomes more marked at $j_i > 50\hbar$, energy constraint is expected to reduce the value of b_n^{max} below the HBL value found in fits to data [6].

Table 1. Comparison of b_n^{max} values for Li_2–rare-gas systems calculated from the E-conservation relation with those obtained from fitting experimental data and reported in [6].

Collision system	b_n^{max} calc	b_n^{max} fit
Li_2–Ne	0.65	0.66
Li_2–Ar	0.59	0.71
Li_2–Xe	0.53	0.56

The values of (E-constrained) b_n^{max} calculated as just described compare well with the b_n^{max} parameters extracted from the AM analysis of experimental data on these systems [6]. Comparisons with $A\,^1\Sigma$ Na_2–Xe, the other E-constrained case found by Osborne and McCaffery [6], are less precise though the experimental data upon which the fits were based are less extensive than for the Li_2 experiments. Table 1 shows values of b_n^{max} obtained by Osborne and McCaffery [6] and those calculated as just described. In practical terms the agreement is sufficiently good that the AM theory may be extended to systems where, for reasons of energy constraint, the full HBL torque arm is not utilized, i.e. light diatomic–heavy collision partner encounters. The AM theory of RT may therefore be used in all cases of RT involving diatomic molecules and, as illustrated below, in certain circumstances, for polyatomics also.

4. State-to-state processes in reactive collisions

We have demonstrated recently [2] that the methods of quantized momentum mechanics may be used to rationalize state-resolved distributions of vibrational and rotational states in atom–diatom and atom–polyatomic molecule *reactive* collisions. The basic principles of the method change relatively little from those used to calculate distributions in inelastic processes. Linear momentum of relative motion, together with that resulting from the enthalpy released or taken in, is converted to momentum of vibration or angular momentum of rotation of the product diatomic molecule by quantized *vector* relations. A significant change, however, is that the distribution function of the effective impact parameter b_n is taken to be sharply peaked and to be close to HBL of the *product* diatomic.

The number of reactive collision systems for which extensive final v, j-resolved populations have been measured is more limited than for the case of inelastic collisions. Three systems for which experimental data exist are illustrated in figure 4 where the E-, $(E + A)$- and A-conservation relations are plotted. The complications that arise from $j_i \neq 0$ are avoided in the case of reactive processes since the product species is initially non-rotating, though as emphasized in [2], rotational and/or vibrational excitation of the *reactants* must be properly accounted for. The plots in figure 4 demonstrate that each of the systems considered falls in the AM-constrained regime for the $v = 0$ rotational values. Again we note explicitly that the A- (and the $E+A$-) constraint relations contain assumptions regarding the magnitude of the effective torque arm.

The plots showing the AM constraint in this system demonstrate why the QMM approach is successful in predicting the outcome of atom–molecule reactive collisions [2]. The implication of this analysis is that provided the constraint plots are such that the A-conservation relation is in effect the constraining process, then the QMM method can give a reliable account of the product quantum state distributions and could, in principle, be used to predict the state distributions in unknown reaction systems. The reactions considered here all are AM constrained for the case that the product species are not vibrationally

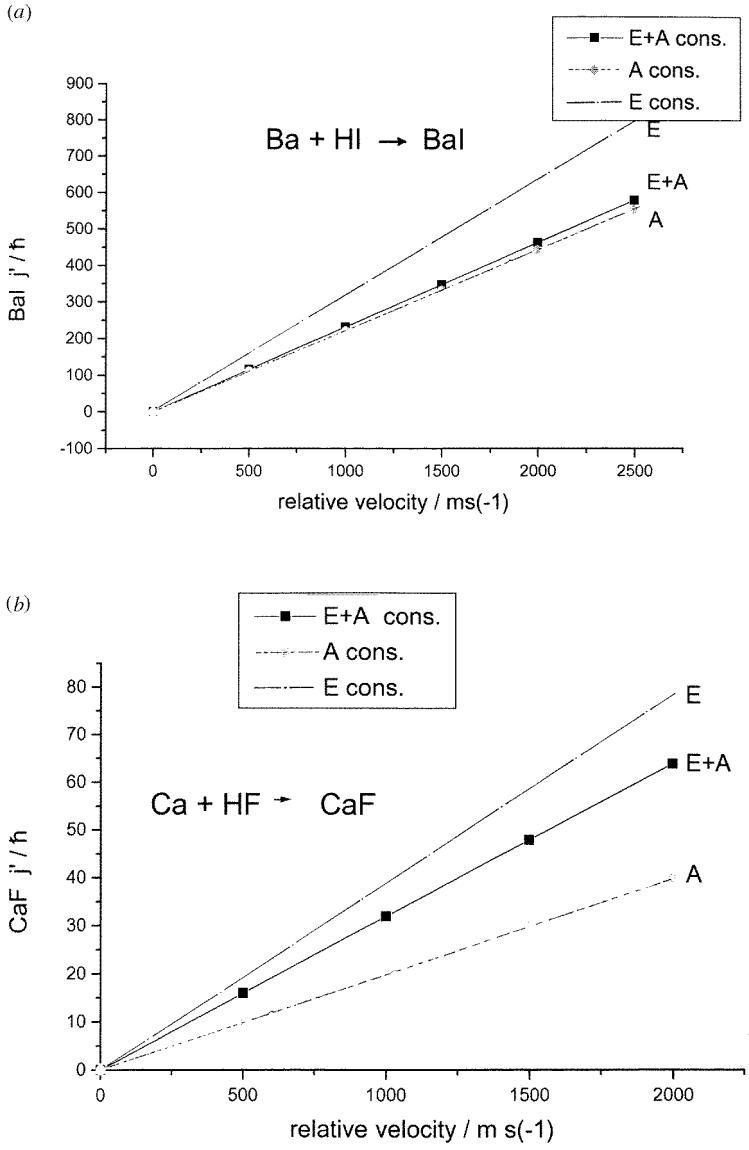

Figure 4. Plots as in figures 1 and 3 but now the systems are reactive and the j' values refer to the *product* species. (*a*) is for BaI product from the reaction Ba + HI and here the value of b_n^{max} utilized was that obtained from analysis of experimental data [2]. (*b*) is for CaF from Ca + HF and (*c*) for HF products from $F + H_2$. All systems are AM constrained and this is particularly marked in (*c*). As discussed in [2], the AM relation using the b_n^{max} values employed here accurately reproduce experimental j' distributions.

excited. We consider the effect of vibrational excitation in further publications. The systems considered do not represent all types of atom–molecule exchange reactions but there are clear kinematic criteria under which the approach we have outlined in [2] may confidently be applied [17].

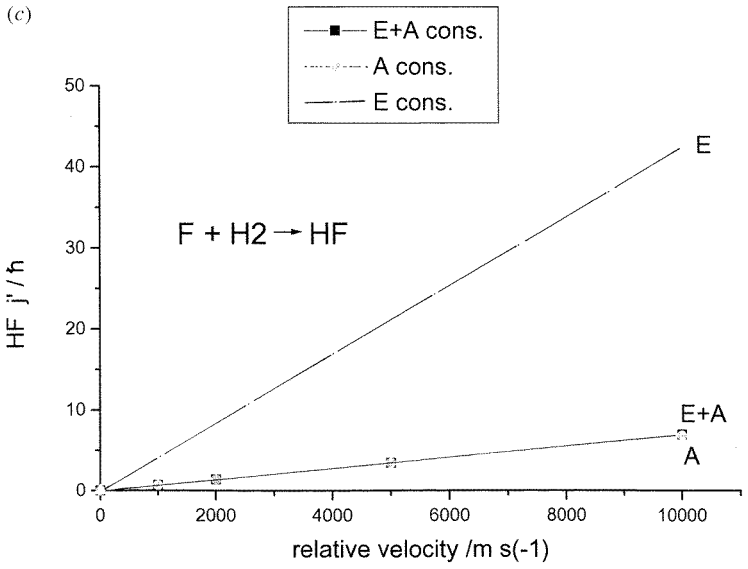

Figure 4. Continued.

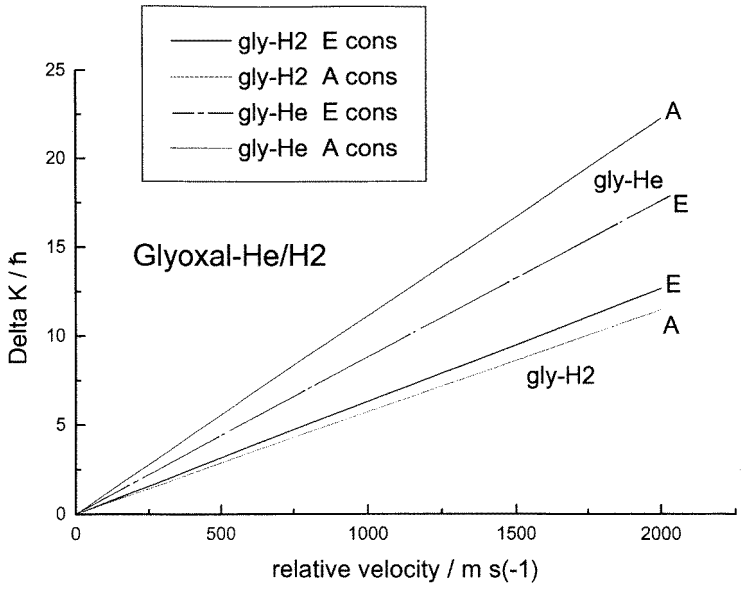

Figure 5. Plot of relative velocity versus ΔK for collisions of H_2 and He with the near symmetric top molecule glyoxal. Calculations are for transitions to $K = J$ levels and hence represent AM generated along the principal axis by collisions in a plane perpendicular to this axis. Note that for H_2 collisions the system is AM constrained but for He and all heavier collision partners, the system is *energy* constrained. This leads to a reduction in b_n^{max} and to RT probabilities as discussed in the text. The new maximum b_n and ΔK values in these circumstances are as predicted in table 2.

5. Atom–polyatomic molecule inelastic collisions

The work of Flynn and colleagues on CO_2–hot atom collisions [8] has demonstrated that linear polyatomics behave rather like elongated diatomics and readily lend themselves to kinematic methods. More daunting are the nonlinear polyatomics since, in general, there is more than one axis about which AM may be generated and the rotational energy becomes strongly dependent on the *direction* of the AM vector in the molecule frame. However, provided the data set considered constitutes AM that does not change direction markedly in the molecular frame on collision, quasi-diatomic conditions apply and the analysis we have outlined above may be carried out. We illustrate the method using data of $|JK\rangle$-resolved RT in the near-symmetric top molecule glyoxal. Clegg *et al* [18] have reported RT measurements of glyoxal in collision with a wide range of partners and have found that the data sets are remarkably similar, the collision reduced mass being the most influential factor in determining the relative distributions of collisional population of the K channels.

This finding would be anticipated from the AM theory of RT [5] in which the quantized vector kinematics off the repulsive wall of the intermolecular potential determine collision outcomes. The dimensions of the repulsive potential vary little with collision partner and primarily reflect the geometry of the molecule concerned. In the AM model, the distribution of final AM states results from a convolution of the probability density of the repulsive anisotropy with that of the relative velocity of collision. As the former of these is principally determined by the topology of the molecule, variation with collision partner will generally reflect the variation of relative velocity distribution in which the reduced mass plays the principal role. This has been noted in a recent report by Parmenter and co-workers [19].

We have shown [20] that symmetric and asymmetric rotor RT is considerably more complex than that involving diatomics, since there is more than one molecular axis about which AM may be generated. In symmetric rotors this is manifested as the magnitude of the K quantum number relative to J while in asymmetric rotors this information is contained in the Jk_ak_c formalism. The process is readily conceived in terms of the AM *sphere* which plots classical trajectories in AM space [20]. The RT process can be envisaged as collision-induced hops from one trajectory to another either within one sphere (or j value) or between spheres. We have demonstrated that RT in the asymmetric rotor may be resolved into components along inertial axes which are induced by collisions in a plane that is perpendicular to the direction of AM change [21].

The data of Clegg *et al* [18] separate collision-induced transitions along the molecular a-axis from those which involve the tilting of the AM vector in the molecule frame. Thus the RT data reported [18] for glyoxal results from collisions occurring in a plane *perpendicular* to the principal axis. A hard-sphere model of this molecule yields a torque arm length of 1.35 Å perpendicular to the a-axis and this value may be used to generate plots of the kind described in the first section for diatomic molecules.

The results of this analysis is shown in figure 5. It is immediately apparent for the most part, glyoxal rare-gas RT is in the *energy*-constrained regime. In all cases other than H_2 as collision partner, the E-conservation relationship is the *slowest* at converting velocity of relative motion into rotational AM. Using the method described above the reduced values of b_n^{max} needed to meet E-conservation for each of the collision systems may be readily calculated. It is evident from the form of the equations used in calculating probability distributions of final j (K in this case) states in the AM theory of RT [5] that reduction of the b_n^{max} parameter would lead to a proportionate 'scaling down' of RT probabilities. This will be addressed more quantitatively in forthcoming reports. The topological features of the glyoxal molecule might be expected to yield a ΔK distribution which is less smooth

Table 2. b_n^{max} values calculated for collision-induced ΔK transitions in glyoxal with the rare gases. The final column shows predicted maximum ΔK values in the experiment.

Rare gas	b_n^{max} calc	ΔK max
H_2	1.35	12
He	1.35	18
Ne	0.74	27
Ar	0.59	31
Kr	0.5	37
Xe	0.46	39

than found in the diatomic case. Table 2 summarizes the results of our calculations of b_n^{max} for glyoxal with the rare gases and subsequent predictions of maximum ΔK values. We anticipate that this could be the basis of a quantitative predictive approach to polyatomic RT.

6. Conclusions

We have demonstrated that the process by which collision energy is converted to rotational energy and that by which relative momentum is converted to rotational angular momentum have different dependences on the relative velocity of collision. Here our focus is on the second of these, the *controlling* mechanism of RT, under constraints set by the first process. We illustrate the kinematic relationships of the conversion process in inelastic and reactive collisions and develop further the quantum-constrained kinematic model of collision-induced state change through which the outcome of collisional events may be predicted. The model emphasizes the importance of threshold or channel opening conditions and we illustrate this in graphs of the threshold velocity in the limiting cases of energy conservation, of angular momentum conservation and of simultaneous energy and angular momentum conservation for zero recoil. In these latter two instances, the effective impact parameter b_n^{max}, is taken to be the half bond length of the target molecule in inelastic processes, of the product molecule in reactive collisions and an equivalent hard-shape distance in the case of the glyoxal molecule.

Plots of these three interconversion functions (equations (5)–(7)) are illustrated for a number of cases for which experimental data exist and the influence of AM and of energy constraints noted. The AM constraint is characterized by a rapid fall-off of RT probability when the available linear momentum is insufficient despite the availability of collision energy. This is found in heavy diatomic–light collision partner systems. The energy constraint is found for light diatomics in collision with heavy collision partners and a reduction in b_n^{max} below HBL may result. This reduced value may be predicted from a simultaneous solution of the E- and the A-conserving relationships for the lowest value of j' (Δj or ΔK) and thus the predictive AM theory of RT may be extended to include such systems.

Furthermore, it is apparent that these plots may be used to infer scattering patterns using readily available kinematic data. For sharply defined velocity distributions the scattering-angle peak will be well defined and calculations are found to agree well with experimental data. The transition from backward to forward scattering is clearly delineated in these plots and indicates the conditions under which long-lived complexes will be observed. The approach may be readily extended to reactive collisions and to inelastic processes in

polyatomics for data sets that represent AM changes along one of the molecule's inertial axes.

It is of interest to note that rotational state distributions may be predicted from QMM for the case of inelastic and reactive collisions using data readily available and with little in the way of computational resources. Scattering angles may be calculated and are found to reproduce accurately those obtained from experiment. There is little recourse to the potential except insofar that molecular size contains usable information on the zero contour of the intermolecular potential, in particular, the repulsive anisotropy. Prediction of probability distributions of j' [5, 6] requires only simple representations of radial and angular dependence of the repulsive potential.

Acknowledgments

MAO and ZR wish to thank EPSRC for studentships. We thank Professor C Parmenter and Dr S Clegg for data on glyoxal–rare-gas RT prior to publication and for helpful comments.

References

[1] McCaffery A J and Wilson R J 1996 *Phys. Rev. Lett.* **77** 48
McCaffery A J and Wilson R J 1997 *J. Phys. B: At. Mol. Opt. Phys.* **30** 5773
[2] McCaffery A J, Truhins K and Whiteley T W J 1998 *J. Phys. B: At. Mol. Opt. Phys.* **31** 2023
[3] Case D A, McClelland G M and Herschbach D R 1978 *Mol. Phys.* **35** 541
[4] Bosanac S D 1992 *Z. Phys.* D **24** 325
Bosanac S D 1993 *Z. Phys.* D **28** 195
Bosanac S D 1993 *J. Phys. A: Math. Gen.* **26** 5523
[5] McCaffery A J, AlWahabi Z T, Osborne M A and Williams C J 1993 *J. Chem. Phys.* **98** 4586
[6] Osborne M A and McCaffery A J 1994 *J. Chem. Phys.* **101** 5604
[7] Derouard J and Sadheghi N 1981 *J. Chem. Phys.* **74** 3324
[8] See, for example, Hershberger J F, Hewitt S A, Sarkar S K, Flynn G W and Weston R E 1989 *J. Chem. Phys.* **91** 4636 and references therein
[9] Kalogerakis K and Zare R N 1996 *J. Chem. Phys.* **104** 7947
[10] Bosanac S 1980 *Phys. Rev.* A **22** 2617
[11] Marks A J 1994 *J. Chem. Soc. Faraday Trans.* **90** 287
[12] Whiteley T W J and McCaffery A J 1996 *J. Phys. B: At. Mol. Opt. Phys.* **29** 6133
[13] Hoffbauer M A, Burdenski S, Giese C F and Gentry W R 1983 *J. Chem. Phys.* **78** 3832
[14] Schiffman A and Chandler D W 1995 *Int. Rev. Phys. Chem.* **14** 371
[15] Levine R D and Bernstein R B 1987 *Molecular Reaction Dynamics and Chemical Reactivity* (New York: Oxford University Press)
[16] Scott T P, Smith N and Pritchard D E 1981 *J. Chem. Phys.* **74** 3324
[17] Truhins K, McCaffery A J and Whiteley T W J in preparation
[18] Clegg S M, Burrill A B and Parmenter C S 1998 *J. Phys. Chem.* submitted
[19] Parmenter C S, Clegg S M, Krajnovitch D J and Lu S P 1997 *Proc. Nat. Acad. Sci., USA* **94** 8387
[20] AlWahabi Z T, Besley N A, McCaffery A J, Osborne M A and Rawi Z 1995 *J. Chem. Phys.* **102** 7945
[21] Truhins K, McCaffery A J, AlWahabi Z T and Rawi Z 1997 *J. Chem. Phys.* **107** 733